International Journal of Fracture **90:** 287–298, 1998.

An analysis of chipping in brittle materials

W.C. CHIU, M.D. THOULESS and W.J. ENDRES
Department of Mechanical Engineering & Applied Mechanics, University of Michigan, Ann Arbor, MI 48109, U.S.A.; e-mail: weichong@engin.umich.edu, thouless@engin.umich.edu, endres@engin.umich.edu

Received 28 October 1997; accepted in revised form 5 March 1998

Abstract. The chipping process in a brittle material subjected to a uniformly applied edge load has been investigated. The present analysis extends earlier work by recognizing that as the chip is formed it may bend and change the loading at the crack tip. This geometry change introduces a nonlinear effect and has significant influence on the phenomenon. The nonlinear effect was demonstrated by incorporating it into an analytical model for a crack propagating along an interface parallel to the free surface. A finite-element analysis was then conducted to examine the crack trajectory formed in a homogeneous material. This numerical analysis showed that the crack reaches a maximum depth, and then deviates back to the free surface to form a spall. The form of this trajectory results from the additional bending moment acting at the crack tip induced by the bending of the chip and the consequent displacement of the applied load. The length of the spall was found to be approximately proportional to the square root of $\hat{E}d^{5/2}/K_{IC}$, where K_{IC} is the fracture toughness of the material, $\hat{E}$ is the appropriate modulus of the material, and d is the depth over which the edge load is applied.

Key words: Fracture mechanics, spalling, crack trajectory.

1. Introduction

Spalling, in which a crack runs beneath a free surface before breaking through to the surface and forming a chip, occurs in many situations of technological importance, such as flint knapping (Fonseca et al., 1971; Cotterell et al., 1985), indentation (Marshall et al., 1982), failure of layered materials (Hutchinson and Suo, 1992), and in machining. Thouless et al. (1987) studied this problem both experimentally and analytically. The basic problem studied in that paper is illustrated in Figure 1a. A homogeneous, isotropic, elastic plate contains a plane crack of length L, much longer than its depth h beneath the free surface. The region between the crack and the free surface is subjected to a concentrated load per unit thickness P exerted along a line of action, $d/2$ below the surface. This loading configuration is equivalent to the one shown in Figure 1b, where the load P acts along the neutral axis of the segment between the crack and the free surface, in conjunction with a bending moment

$$M = Pe = \frac{P}{2}(h - d) \tag{1}$$

The crack-tip stresses for this class of problem are generally mixed mode and characterized by stress-intensity factors, K_{I} and K_{II} given by (Thouless et al., 1987)

$$\begin{aligned} K_{\mathrm{I}} &= 0.434Ph^{-1/2} + 1.934Mh^{-3/2}, \\ K_{\mathrm{II}} &= 0.558Ph^{-1/2} - 1.503Mh^{-3/2}. \end{aligned} \tag{2}$$

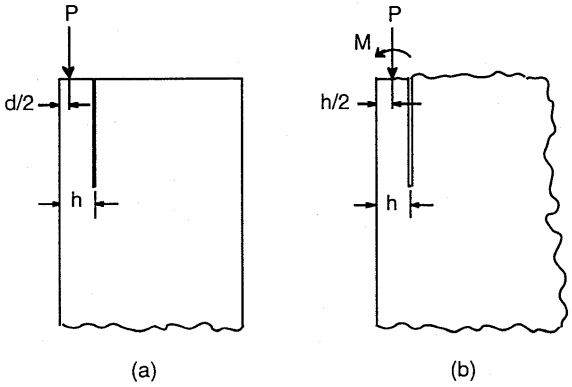

Figure 1. Geometry and loading for edge cracking. The physical configuration is shown in (a), while the idealized configuration is shown in (b). In (b), an eccentric load, P, has been replaced by a load acting along the neutral axis of the segment between the crack and free surface and a bending moment M.

A series of experiments in which sheets of PMMA and glass were subjected to a compressive edge load revealed that, irrespective of the location of initial crack, the crack always followed a steady-state trajectory parallel to the free surface and at a characteristic depth below it (Thouless et al., 1987). The occurrence of a steady-state trajectory was explained with the assumption that the crack followed a trajectory along which $K_{\mathrm{II}} = 0$. Substitution of Equation (1) into (2) shows that, for the geometry shown in Figure 1, $K_{\mathrm{II}} = 0$ when $h = 3.9d$ (Thouless et al., 1987). Furthermore, it was shown that this is a stable trajectory. A crack shallower than this depth will be subjected to a positive value of K_{II} that will tend to drive it deeper; a crack deeper than this will be driven towards the free surface. Comparisons of this predicted steady-state trajectory ($h = 3.9d$) with experimental observations showed a discrepancy. The crack was observed to be somewhat shallower ($h \approx 2.5d$) than predicted. This difference was believed to arise from surprisingly strong effects of the other free surface (Drory et al., 1988; Thouless and Evans, 1990). In the vicinity of the depth where $K_{\mathrm{II}} = 0$, K_{II} has a fairly mild gradient with respect to depth. Small changes in K_{II} can have a large influence on the depth at which $K_{\mathrm{II}} = 0$ (Hutchinson and Suo, 1992). Subsequent work showed that identical mechanics apply when a film under a state of residual tension delaminates from a brittle substrate. Provided the substrate is not too tough, the film can delaminate by cracking of the substrate. Again, the crack seeks out a $K_{\mathrm{II}} = 0$ trajectory that is parallel to the free surface (Drory et al., 1988; Hu et al., 1988). The depth of this trajectory depends on the ratio of the elastic constants of the film and substrate (Drory et al., 1988; Suo and Hutchinson, 1989).

A major difference observed experimentally between delamination of a film and cracking of a plate loaded by an externally applied compressive force was that, in the latter case, the subsurface crack tended to leave the predicted steady-state trajectory, deviating towards the free surface and forming a spall (Thouless et al., 1987). This spalling is observed anytime a glass or ceramic plate is hit upon its edge. Thouless et al. (1987) hypothesized that spalling occurs when the material between the crack and the free surface buckles under the applied load. Swensen and Kaushik (1990) used a finite-element analysis to follow the trajectory of an edge crack, and suggested that spalling could be caused by the crack approaching a fixed boundary. However, with these two exceptions the work in this area has predominately concentrated on cracking associated with residual stresses, rather than with applied loads. Therefore the issue of chip formation has not been fully resolved. In the present work, prompted by an interest

in the mechanics of machining brittle materials, this question is revisited. An analytical result for delamination along a weak interface is presented first to illustrate the principles involved. This is followed by a finite-element study of cracking in homogenous materials in which cracks are followed from their initial position through to spalling. These studies permit results for the geometry of spalls to be determined in terms of the material properties and the depth below the surface at which an axial load is applied.

2. Non-linear effects on crack growth

The bending moment induced on the arm between the crack and the free surface by the eccentric nature of the load (Equation 1) will cause the arm to bend, unless it is restrained by a force normal to the crack surface. If crack growth is driven by the relaxation of residual tension in a coating, this deformation has no effect on the mechanics of the problem. The equations given in Thouless et al. (1987) for the homogeneous case, and the equivalent equations for bimaterial problems (Suo and Hutchinson, 1989) are then always appropriate, and a steady-state crack trajectory is anticipated. However, the situation is very different if the load arises from an applied external force, as in a machining or an indentation process. As the beam deforms, the point of application of the load may move, and the effective bending moment acting on the crack tip may change. Even if the load is constrained from moving, the lateral force imposed by this constraint will also change the effective bending moment. In either case, it can be seen from Equation (2) that this change in the bending moment will affect the mode-mixedness of the crack-tip stress field. The linear solution obtained by substituting Equation (1) into (2), in which the mode-mixedness depends only on P, d and h, is valid only when the applied load is very low. At higher loads, geometrical nonlinear effects become important.

The nonlinear behavior is illustrated analytically in this section by considering the elastically homogeneous problem shown in Figure 1, but assuming the crack is confined to an interface that is located at a fixed distance h beneath the free surface. A force (per unit thickness) of magnitude P is applied at a distance $d/2$ below the free surface, and the crack is of length L. Assuming that the point of application of the load is free to rotate, the resultant bending moment acting at the crack tip is given by (Gere and Timoshenko, 1997)

$$M = Pe + Py_{\max} = Pe \sec\left(\sqrt{\frac{P}{\hat{E}I}}L\right), \tag{3}$$

where e is the eccentricity of the load, $\hat{E} = E$ for plane stress and $\hat{E} = E/(1-\nu^2)$ for plane strain, E is the modulus of the material, ν is Poisson's ratio, and $\mathrm{I} = h^3/12$. Upon substituting Equation (3) into (2) and normalizing, nonlinear expressions for the crack-tip stress-intensity factors can be obtained in terms of P:

$$\frac{K_{\mathrm{I}}}{\hat{E}\sqrt{d}} = 0.435\left(\frac{P}{\hat{E}d}\right)\left(\frac{h}{d}\right)^{-1/2} + 0.996\left(\frac{P}{\hat{E}d}\right)\left(\frac{h}{d}\right)^{-1/2}\left[1-\left(\frac{h}{d}\right)^{-1}\right] \times \sec\left[2\sqrt{3}\left(\frac{P}{\hat{E}d}\right)^{1/2}\left(\frac{h}{d}\right)^{-3/2}\left(\frac{L}{d}\right)\right],$$

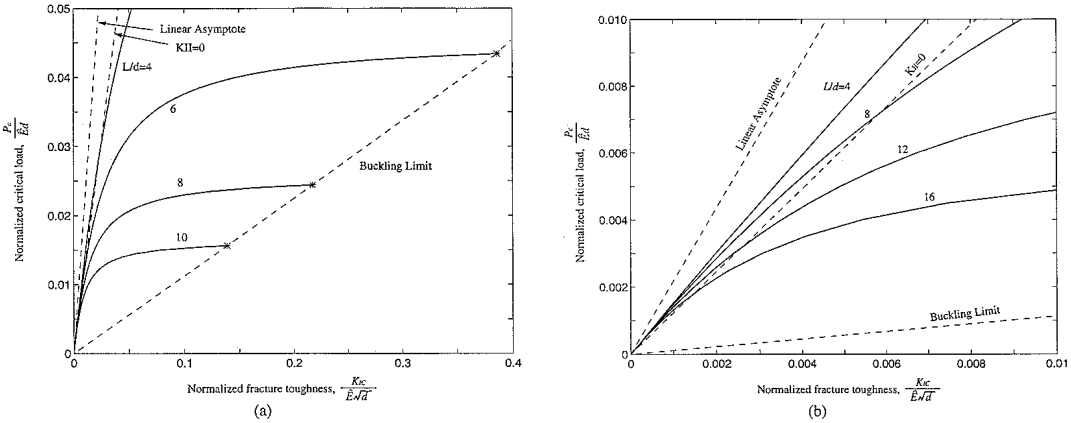

Figure 2. Critical load required for crack propagation plotted as a function of the normalized fracture toughness of the material, for different crack lengths. The crack is assumed to be on a plane trajectory fixed at a depth $h = 2d$ below the free surface, where $d/2$ is the point of application of the load. The linear limit, $K_{\mathrm{II}} = 0$, and the buckling limit are noted on this figure. (b) shows an enlarged view of (a).

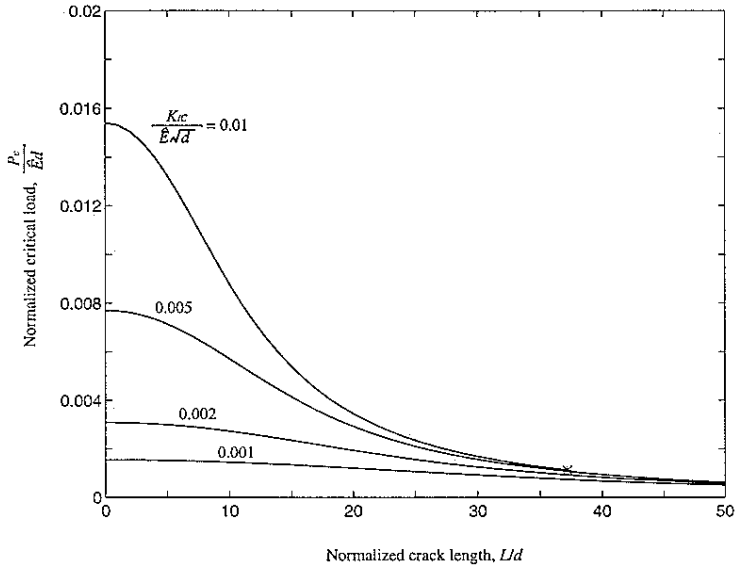

Figure 3. Critical load required for crack propagation plotted as a function of crack length for different values of the normalized fracture toughness. The crack is assumed to be on a plane trajectory fixed at a depth $h = 2d$ below the free surface, where $d/2$ is the point of application of the load. The symbol $(*)$ indicates the buckling limit for $K_{Ic}/\hat{E}\sqrt{d} = 0.01$.

$$\frac{K_{\mathrm{II}}}{\hat{E}\sqrt{d}} = 0.558\left(\frac{P}{\hat{E}d}\right)\left(\frac{h}{d}\right)^{-1/2} - 0.753\left(\frac{P}{\hat{E}d}\right)\left(\frac{h}{d}\right)^{-1/2}\left[1-\left(\frac{h}{d}\right)^{-1}\right] \times \sec\left[2\sqrt{3}\left(\frac{P}{\hat{E}d}\right)^{1/2}\left(\frac{h}{d}\right)^{-3/2}\left(\frac{L}{d}\right)\right]. \tag{4}$$

Two features can be noticed immediately from these equations. First, in contrast to Equation (2), the mode-mixedness depends on the crack length. Second, if a failure criterion of the form $K_{\mathrm{I}} = K_{IC}$ (where K_{IC} is the mode-I fracture toughness of the interface) is assumed, the force that must be applied to cause fracture decreases as the crack grows. Using this failure criterion, it is possible to plot the normalized critical load for fracture $P_c/\hat{E}d$ as a function of the normalized material properties $K_{\mathrm{IC}}/\hat{E}\sqrt{d}$ for various crack lengths (Figure 2). This figure contains three characteristic lines. The linear solution obtained from Equations (1) and (2) provides an asymptote for the critical load that is appropriate for very low loads. The buckling limit represents the limit at which the load required to continue delamination exceeds the maximum load that can be supported by the material between the interface and free surface without buckling. The third line represents the condition $K_{\mathrm{II}} = 0$. Combinations of load and crack length that lie above this line correspond to conditions where $K_{\mathrm{II}} > 0$. This means that the crack will tend to deviate down into the substrate. Points below this line correspond to conditions where $K_{\mathrm{II}} < 0$, and the crack will try to deviate up to the free surface. If the problem being considered is the delamination of a brittle film by an applied load (such as in the scratch test (Venkatarman et al., 1992), then the $K_{\mathrm{II}} = 0$ line gives the conditions at which spalling may occur. It will be observed that the chip length at which spalling may occur increases as either the toughness of the interface decreases or the modulus of the film increases. In Figure 3, the results are re-plotted to illustrate how the critical load drops as the crack extends along the interface.

3. Finite element analysis

In homogeneous materials with no interface to define the crack trajectory, the crack is free to seek out its own path. Assuming that the initial crack length is small compared to the final spall length L, dimensional analysis shows that L and the maximum depth of the crack h are of the form

$$\begin{aligned} \frac{L}{d} &= F_1\left(\frac{K_{\mathrm{I}c}}{\hat{E}\sqrt{d}}\right), \\ \frac{h}{d} &= F_2\left(\frac{K_{\mathrm{I}c}}{\hat{E}\sqrt{d}}\right). \end{aligned} \tag{5}$$

A finite-element analysis is required to determine the functions F_1 and F_2. A commercial, multipurpose finite-element package, ABAQUS, was used. The model consisted of a plate, constrained by simply-supported boundaries on the bottom and on one end. The top surface and the other edge were free. Linear elasticity was assumed, and quadratic-order, isotropic, plane-strain elements were used for the mesh. A uniform compressive load was applied in a normal direction to a portion of the edge of the plate above some initial crack. The absolute direction of this load was kept constant as the crack propagated. A sensitivity analysis demonstrated that the dimensions of the plate were sufficiently large to ensure that the boundaries had a negligible effect on the cracking. A series of calculations were performed with different values of $K_{\mathrm{IC}}/\hat{E}d$ to investigate the influence of this parameter on the crack trajectory.

To begin the analysis, an initial crack of length $d/5$ and parallel to the top surface was introduced at the edge of the plate (Figure 4). The mode-I and mode-II stress-intensity factors, K_{I} and K_{II}, were determined by a crack-opening-displacement method combined with the use of collapsed quarter-point-elements (chosen for their capability of capturing the stress-strain

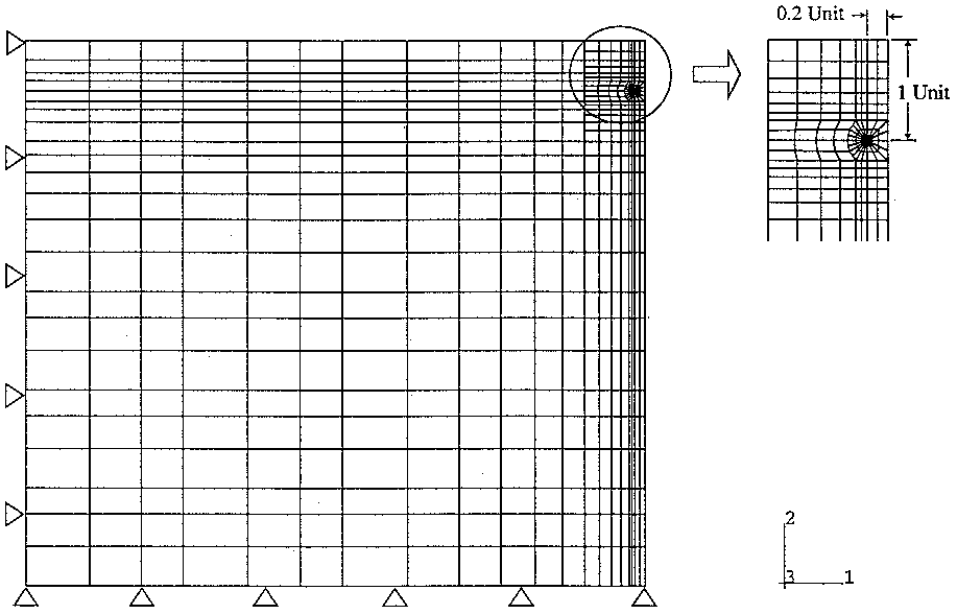

Figure 4. Initial finite-element mesh used for analyzing the edge-crack problem.

singularity at the crack tip (Shih et al., 1976; Murti et al., 1985)). The computed values of K_{I} and K_{II} were used to determine the direction of the maximum hoop stress with respect to the orientation of the original crack tip. This direction,

$$\theta_c = 2\tan^{-1}\left\{\frac{1}{4}\left[\frac{K_{\mathrm{I}}}{K_{\mathrm{II}}} \pm \sqrt{\left(\frac{K_{\mathrm{I}}}{K_{\mathrm{II}}}\right)^2 + 8}\right]\right\}, \tag{6}$$

was taken to be the direction for any new increment of crack growth. The condition for incremental crack extension along this new direction was determined using the analysis of Cotterell and Rice for a kinked crack (Cotterell and Rice, 1980). From this analysis the local mode-I stress-intensity factor, k_1, at the tip of a small kink inclined at an angle θ_c to a crack tip subjected to global stress-intensity factors, K_{I} and K_{II}, is given by

$$k_1 = \frac{1}{4}\left(3\cos\frac{\theta_c}{2} + \cos\frac{3\theta_c}{2}\right)K_{\mathrm{I}} - \frac{3}{4}\left(\sin\frac{\theta_c}{2} + \sin\frac{3\theta_c}{2}\right)K_{\mathrm{II}}. \tag{7}$$

The kink was assumed to form when k_1 reached a value K_{IC}, the fracture toughness of the material. The size of the kink chosen for each step of the calculation depended on the magnitude of θ_c. When this angle was large, the size of the kink was kept small so as to capture the details of the crack trajectory. When the change in angle was small, a larger increment in crack growth was chosen. The precise criterion for determining each increment of crack length depended upon the results of the analysis and upon the experience developed during the simulations. After each new increment of crack growth had been established, the model was then remeshed to describe the new configuration with an extended crack, and the analysis was repeated.

To demonstrate the validity of the algorithm, a linear analysis was performed using the model and procedure described above. A unit load was applied at each incremental step of

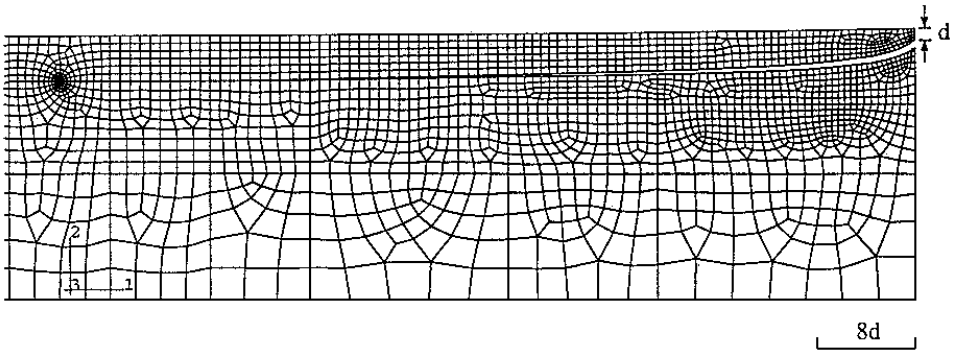

Figure 5. Crack path obtained using a linear analysis. The figure shows the trajectory and the mesh used just after the crack has entered the steady-state.

crack growth to obtain the ratio of $K_{\mathrm{I}}/K_{\mathrm{II}}$ used for calculating the crack-growth direction. Figure 5 shows the crack path obtained using this linear analysis. It can be observed that the initial crack propagates down from the free surface and reaches a steady-state trajectory. The nondimensional load, $P/K_{\mathrm{I}c}\sqrt{h}$, where h is the maximum crack depth, required to cause the crack to propagate along this trajectory was determined to have a value of 0.88. This is essentially identical to the analytical result, 0.87, found for a quarter plane (Thouless et al., 1987). The numerical calculations predicted a nondimensional crack depth, h/d of 3.64. This is quite close to the analytical result of 3.9 (Thouless et al., 1987). The small differences between the analytical solution and the finite-element results are probably caused by the finite geometry of the numerical model, since it has been shown that the depth at which $K_{\mathrm{II}} = 0$ is very sensitive to the size of the specimen (Hutchinson and Suo, 1992; Drory et al., 1988).

When nonlinear effects were included in the numerical analysis, additional computational steps were needed. At each increment of crack growth, the ratio of $K_{\mathrm{I}}/K_{\mathrm{II}}$ and, thus, the crack propagation angle no longer depended only on the crack geometry; it also depended on the magnitude of the applied load. Therefore, at each step in the analysis, the load was incrementally increased from zero. For each load increment, the values of K_{I} and K_{II} were computed to determine the angle at which a kink would form and what the magnitude of the local mode-I stress-intensity factor k_1 at the tip of such a kink would be. If k_1 was less than K_{IC} then the load was incremented, and the analysis repeated for the same crack geometry. When $k_1 = K_{IC}$, the crack was incrementally advanced, and the model re-meshed. The results of this analysis are presented in the following section. In addition to examining the effects of nonlinearity on the crack trajectory, the influence of the nondimensional parameter $K_{\mathrm{I}c}/\hat{E}\sqrt{d}$ on cracking was also investigated.

4. Results and discussion

The crack trajectories corresponding to three different values of the nondimensional parameter $K_{\mathrm{I}c}/\hat{E}\sqrt{d}$ are shown in Figure 6. The crack is initially driven down from the free surface, following the same trajectory as for the linear analysis. As the deformation of the arm increases, the nonlinear effect starts becoming important as the bending moment acting on the crack tip increases. This causes the crack trajectory to move closer to the free surface than predicted from the linear analysis. The effect becomes more marked as the crack grows, and eventually the crack returns to the free surface to form a spall. It is important to emphasize that it was

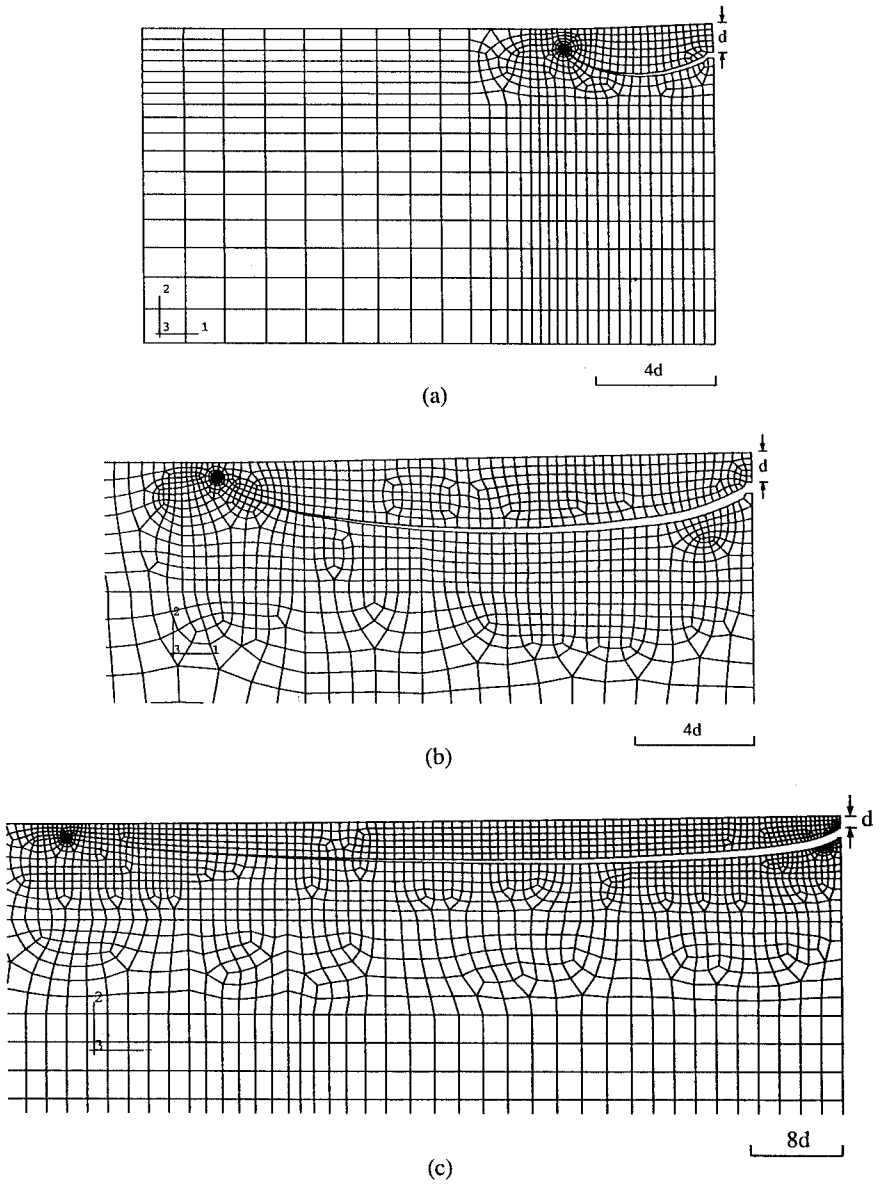

Figure 6. Crack trajectories for three different values of $K_{Ic}/\hat{E}\sqrt{d}$: (a) 2.0×10^{-2}, (b) 2.0×10^{-3} and (c) 2.0×10^{-4}.

verified that the deflection of the crack was not influenced by the presence of any boundaries This is in contrast to the studies described in (Swenson and Kaushik, 1990) where the cracks approached a boundary, and then deviated towards the free surface.

The characteristics of these trajectories are shown in Figures 7 and 8. Figure 7 shows how the length of the spall increases as the parameter $K_{Ic}/\hat{E}\sqrt{d}$ decreases. It has previously been proposed that the spall length is dictated by a buckling condition. It was suggested that the crack would grow for an extended distance along the steady-state trajectory and then, when the buckling condition was met, the crack would deviate to the free surface and form a spall. This would result in a nondimensional spall length, L/d, that is inversely proportional

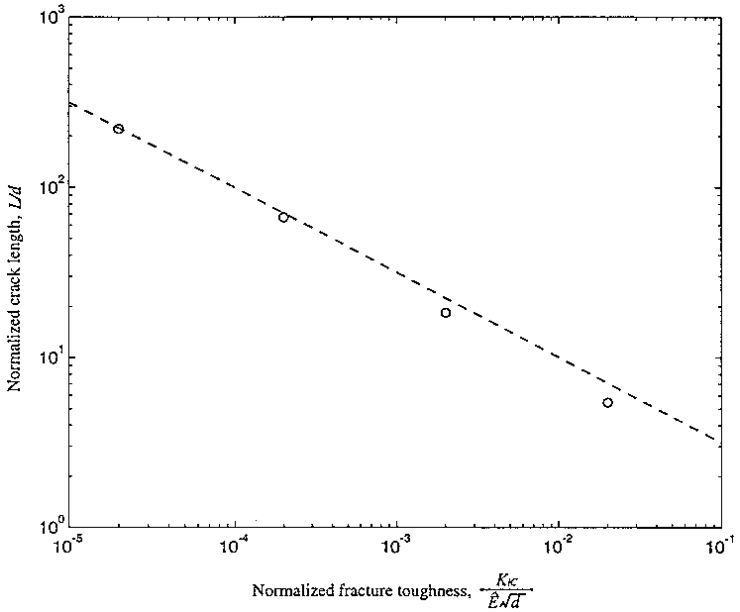

Figure 7. Normalized length of spall as a function of $K_{\mathrm{I}c}/\hat{E}\sqrt{d}$, obtained from the finite-element analyses. The asymptotic line indicates a slope of $-1/2$.

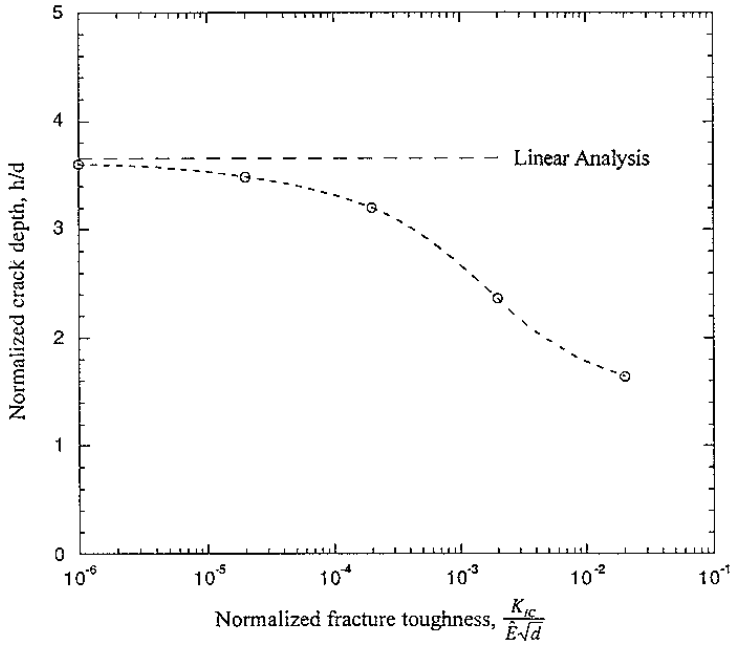

Figure 8. Normalized value of the maximum depth of spall as a function of $K_{\mathrm{I}c}/\hat{E}\sqrt{d}$.

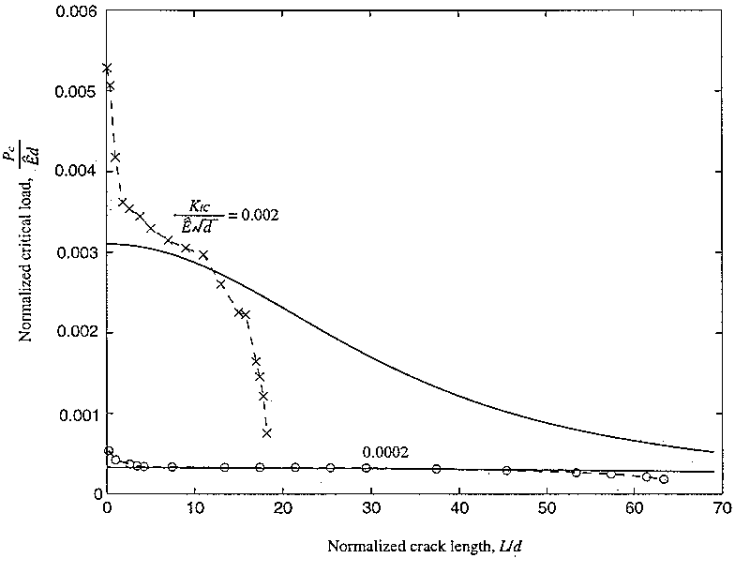

Figure 9. Critical load required for crack propagation plotted as a function of crack length for different values of $K_{Ic}/\hat{E}\sqrt{d}$. The analytical results of Equation (2) (using a crack depth approximately corresponding to the maximum depth obtained by the finite-element analysis) have been superimposed on this plot.

to $(K_{Ic}/\hat{E}\sqrt{d})^{1/2}$ (Thouless et al., 1987). Figure 7 demonstrates that the numerical results closely follow this trend, especially as $K_{Ic}/\hat{E}\sqrt{d}$ decreases. However, as can be seen by a comparison between Figure 7 and Figure 2, the spall lengths are considerably shorter than would be predicted from such a buckling analysis. Although the crack trajectory may reach an approximate steady-state depth, the crack never really grows parallel to the free surface, and it starts coming back up to the free surface before the buckling conditions are met.

Figure 8 shows how the maximum depth of the crack varies with the nondimensional parameter $K_{Ic}/\hat{E}\sqrt{d}$. When this parameter is large, so either a large force needs to be applied to cause crack growth or the material is very compliant, the nonlinear effect becomes important even for very short cracks. Consequently, the crack deviates back towards the free surface at relatively short lengths, resulting in a shallower maximum depth. As the magnitude of the nondimensional parameter decreases, the nonlinear effect becomes important for longer cracks and the crack follows the linear trajectory further. As shown in Figure 8, the maximum depth of the crack then becomes asymptotic to the depth of the linear steady-state solution as $K_{Ic}/\hat{E}\sqrt{d}$ approaches zero.

Edge-loading experiments on PMMA specimens were described in (Thouless et al., 1987). The shape of the spalls observed in that work were very similar to those predicted here. However, the spall length was much longer than predicted by the present analysis. This difference probably arises because the specimens were loaded by a plate that exerted a lateral frictional force and partially restrained the deformation of the chip. Further numerical analyses are currently being performed to explore the effect of lateral forces on the chipping phenomenon, with a particular interest on investigating how friction and rake angles of cutting tools might affect the crack path. It should be noted that even if the lateral constraint is sufficiently large to prevent any lateral motion of the applied load, the crack trajectory is not expected to be the same as predicted by the linear analyses developed previously. The lateral force will impose an additional bending moment at the crack tip that will affect the mode-mixedness.

Figure 9 shows how the load required to propagate a crack is predicted to vary with crack length. Superimposed on this plot is the analytical solution for the load (Equation 4) for cracks growing at the appropriate depths. It will be observed that when the crack is short, the load drops very quickly from a maximum value to a value approximately described by the analytical result. Eventually, when the crack trajectory starts deviating quickly towards the free surface, the load rapidly drops to zero.

5. Conclusions

Previous analyses of cracks propagating parallel to a free surface have neglected the nonlinear effects that can be introduced by bending of the material above the crack. These effects have been demonstrated by an analytical model for crack growth along an interface driven by an externally applied compressive load. This model illustrates how the nonlinear effect becomes important as the crack length increases and as the nondimensional material parameter $K_{\mathrm{I}c}/\hat{E}\sqrt{d}$ increases. The trends predicted in this model have been confirmed by finite-element calculations exploring spalling in homogeneous materials subjected to a uniform edge load. The numerical analysis demonstrates that while the spalling crack initially follows the linear trajectory that would establish a steady-state crack depth, the nonlinear effect tends to cause the crack to deviate back towards the free surface and to form a spall. The nondimensional spall length L/d is approximately proportional to $(K_{\mathrm{I}c}/\hat{E}\sqrt{d})^{-1/2}$. Further studies are being conducted to examine the effect of a lateral force on the spall, as might be imposed by frictional forces or forces applied at an angle other than normal to the edge. A lateral force would introduce an additional moment at the crack tip that would also affect the mode-mixedness of the problem. Consequently, even if the point of application of the load were not free to move, the effects considered in the present paper are expected to have an influence on chip formation.

Acknowledgments

This work was supported by NSF grant #DMI-9522809.

References

Cotterell, B. and Rice, J.R. (1980). Slightly curved or kinked cracks. *International Journal of Fracture* **10**, 305–321.

Cotterell, B., Kamminga, J. and Dickson, F.P. (1985). The essential mechanics of conchoidal flaking. *International Journal of Fracture* **29**, 205–221.

Drory, M.D., Thouless M.D. and Evans, A.G. (1988). On the decohesion of residually-stressed thin films. *Acta Metallurgica* **36**, 2019–2028.

Fonseca, J.G., Eshelby, J.D. and Atkinson, C. (1971). The fracture mechanics of flint-knapping and allied processes. *International Journal of Fracture Mechanics* **7**, 421–433.

Gere, J.M. and Timoshenko, S.P. (1997). *Mechanics of Materials*, PWS Publishing Co., Boston, MA.

Hu, M.S., Thouless, M.D. and Evans, A.G. (1988). The decohesion of thin films from brittle substrates. *Acta Metallurgica* **36**, 1301–1307.

Hutchinson, J.W. and Suo, Z. (1992). Mixed mode cracking in layered materials. *Advances Applied Mechanics* **29**, 63–191.

Marshall, D.B., Lawn, B.R. and Evans, A.G. (1982). Elastic/Plastic indentation damage in ceramics: The lateral crack system. *Journal of American Ceramic Society* **65**, 561–566.

Murti, V., Valliappan, S. and Lee, I.K. (1985). Stress intensity factor using quarter point element. *Journal of Engineering Mechanics* **111**, 203–217.

Shih, C.F., DeLorenzi, H.G. and German, M.D. (1976). Crack extension modeling with singular quadratic isoparametric elements. *International Journal of Fracture* **12**, 647–651.

Suo, Z. and Hutchinson, J.W. (1989). Steady-state cracking in brittle substrate beneath adherent films. *International Journal of Solids Structures* **25**, 1337–1353.

Swenson D.V. and Kaushik, N. (1990). Finite-element analysis of edge cracking in plates. *Engineering Fracture Mechanics* **37**, 641–652.

Thouless, M.D., Evans, A.G., Ashby, M.F. and Hutchinson, J.W. (1987). The edge cracking and spalling of brittle plates. *Acta Metallurgica* **35**, 1333–1341.

Thouless, M.D. and Evans, A.G. (1990). Comment on the spalling and edge-cracking of plates. *Scripta Metall. Mater.* **24**, 1507–1510.

Venkataraman, S., Kohlstedt, D.L. and Gerberich, W.W. (1992). Microscratch analysis of the work of adhesion for Pt thin films on NiO. *Journal of Materials Science* **7**, 1126–1132.